ITC 3/54
Information Technology and Control
Vol. 54 / No. 3/ 2025
pp. 1010-1029
DOI 10.5755/j01.itc.54.3.41742

Forest Fire Recognition and Prediction Based on Fully Convolutional Network and Rothermel Model

Received 2025/05/29 | Accepted after revision 2025/07/22

HOW TO CITE: Chen, M., Shi, K., Tan, Y. (2025). Forest Fire Recognition and Prediction Based on Fully Convolutional Network and Rothermel Model. *Information Technology and Control*, 54(3), 1010-1029. https://doi.org/10.5755/j01.itc.54.3.41742

Forest Fire Recognition and Prediction Based on Fully Convolutional Network and Rothermel Model

Mingyi Chen
School of Economics & Management, Shanghai Maritime University, Shanghai, 201306, China
These authors contributed equally.

Kangrong Shi
School of Information Science and Technology, Beijing University of Technology, Beijing, 100124, China
These authors contributed equally.

Yuxin Tan*
College of Artificial Intelligence, North China University of Science and Technology, Tangshan, 063210, China

Corresponding author: 200536@stu.ncst.edu.cn

This paper establishes a combined fire recognition and prediction model to study the spread of forest fires in response to the frequent occurrence of forest hill fires and its difficult recognition and prediction pain point. Based on the traditional recognition neural network, this paper innovatively establishes Fully Convolutional Network (FCN) to improve the fire recognition accuracy. The Rothermel model is introduced for fire spread prediction of the Palisades Mountain Fire in Los Angeles, and it is found that the accuracy of the Rothermel model is as high as 87% and the stability is about 70.9%. Referring to the excellent model performance of the Rothermel model, this paper establishes a combined model for identification and prediction with the combination of FCN and Rothermel in order to improve the accuracy of fire identification and prediction, and provide double accuracy to ensure the reliability of the study. Based on the simulation of forest fires in a simulated wildland environment, the fire spreading stages are segmented into 4 parts, fire recognition is performed by FCN network, and Rothermel fire prediction is performed based on the recognition results. It is found that the combined model effectively reduces the errors of individual models, complements the

advantages of individual models, and improves the fire identification and prediction accuracy. At last, this paper suggests a combination with the field of drones for smart fire prevention and reference.

KEYWORDS: Forest Fire Recognition and Prediction, Fully Convolutional Network, Rothermel Model, FCN-Rothermel Model

1. Introduction

Fire as one of the frequent natural disasters worldwide, poses a serious threat to the safety of human life and property, the balance of the ecosystem and socio-economic development due to its suddenness and destructive nature. In recent years, under the influence of factors such as the intensification of climate change, the acceleration of urban expansion and the expansion of the scope of human activities, the global trend of fire occurrence has shown an increase in frequency and scale[7]. For example, the fires that broke out in the Pacific Palisades area of Los Angeles in 2025 quickly spread to Santa Monica and beyond, overtopping more than 38,000 acres (about 153 square kilometers), twice the size of Manhattan. More than 24 million hectares damaged by Australian hill fires in 2020[19]. The total amount of carbon dioxide released from the Amazon rainforest fires in 2019 amounted to 228 million tons, and such events not only cause direct economic losses, but also have far-reaching impacts on regional ecological recovery and the global carbon cycle. In this context, how to reduce disaster losses through efficient and accurate fire early detection technology, and with the help of scientific spread prediction modeling to provide support for emergency decision-making, has become a key issue to be solved in the field of disaster prevention and mitigation.

In order to carry out an efficient detection of existing fires, Schultze [29] investigated the dynamic behavior of open fires within the scope of the development of a video-based fire detection system using different audio and video systems to record standardized fires and analyze their flow and flickering. Liang [20] proposed an early smoke detection method for forest fires by combining super-resolution reconstruction network and smoke segmentation network. San-Miguel-Ayanz [28] assessed the use of existing remote sensing systems for active fire detection and highlighted the applicability of these systems in fire emergency management and firefighting. Barmpoutis [4] describes the application of optical remote sensing in early fire warning and discusses its system types, detection models, and advantages and disadvantages. Prema [26] proposed a texture analysis method for flames in forest fire detection by segmenting candidate flame regions through YCbCr color space, extracting static and dynamic texture features, and classifying real flames from non-flames using an Extreme Learning Machine classifier. Appana [3] Extraction of temporal features by optical smoke flow pattern analysis and spatio-temporal energy analysis and identification of smoke pixels using HSV color space. Zhao [34] proposed the Fire-YOLO detection model to extend the feature extraction network in three dimensions, which enhances the feature propagation capability for fire small target identification, improves the network performance, and reduces the model parameters. Li [21] proposed a fast and efficient fire detection model based on MobileNetV3 and unanchored structure, the model has better performance and speed on public fire dataset, and is suitable for real-time fire detection and embedded device applications. Wu [32] proposed a multi-scale fire image detection method by combining convolutional neural network (CNN) and Transformer. Abdusalomov [1] presents an improved forest fire detection method to classify fires using a deep learning approach based on a new version of the Detectron2 platform (a scratch rewrite of the Detectron library).

Marziliano [23] proposes the use of mathematical reaction-diffusion models aimed at predicting the development of forest fires. Encinas [11] Proposed Regular Hexagonal Regions for Predicting Fireline Spread in Uniform and Non-Uniform Environments Based on 2D Metacellular Automata Models. Kuznetsov [18] derives a system of differential equations that reliably predicts the span of moist forest fuel belts that provide forest fire contain-

ment at all flame lengths. Mutthulakshmi [24] proposes the application of metacellular automata to predict and analyze the effects of fire suppression intervention strategies, taking into account both the spatial and propagation dynamics of fire. Glasa [13] demonstrated several simple examples of fire propagation that correspond to elliptical and non-elliptical localized fire propagation under uniform conditions. Jing [16] proposed Light Gradient Boosting Machine (LightGBM) model, a powerful prediction algorithm that can handle large-scale data and complex problems. Diaz-Avalos [10] simulated the magnitude of forest fires in Castellón, Spain, from 2001-2006 using a spatial marker-point process, modeling with spatial covariates to capture spatial variability and identify fire-related factors, and Bayesian methods (including INLA and SPDE) for model fitting. Khennou [17] presented the FU-NetCastV2 for fire spread and burned area mapping. Byari [6] Appropriate Multiscale CA Modeling Methods Based on 3D Geometric Cells and the Proposed Methods Applied as Part of the Overall Forecasting System for Predicting the Spread of Wildfires.

In this paper we used fully convolutional network (FCN) to segment the current fire images of the scene, which can effectively improve the accuracy of the prediction; and we introduced the Rothermel model for the prediction of fire spreading trend to verify its performance in simulating fire spreading. Currently, there are various research topics on wildfires that are being addressed and improved to develop more effective mitigation strategies for wildfire impacts. For example, wildfire spread prediction [15], Forecast of wildfire occurrence [31], Active fire detection and fire risk calibration [25]. Rothermel model is the most commonly used model for predicting fire spread rates [35]. One of the Rothermel models proposed by Glasa et al. [13] defines the shape of the fire as a double ellipse. Another model defines the shape of the fire as a single ellipse. Edigley et al. [12] used a two-stage prediction scheme for the input data describing the fire scenarios in a forest fire simulation model to adjust the unknown parameters to reduce the elevated level of uncertainty that exists in the input data for the fire scenarios. Based on this, this paper draws on the improved method of Rothermel model in the previous literature to analyze the fire spread prediction in combination with real cases. The Rothermel model also is introduced to predict the fire spread trend and verify its performance in simulating fire spread.

The main contributions of this paper are as follows:

1. Due to the uncertainty of fire spread and the errors associated with fire remote sensing identification techniques, it is crucial to upgrade and innovate traditional neural networks. Based on the traditional recognition neural network method, the innovative establishment of Full Convolutional Network (FCN) to improve the accuracy of fire recognition. With the deep residual network, RESNet, as the backbone, FCN incorporates the Conv Block and Identity Block, to recognize the flames of different color images in remote sensing technology while maintaining robustness, which is a major improvement over the traditional deep learning networks.
2. Since fire spread is affected by multiple factors, its effect needs to be quantified. Rothermel model can be used for fire spread prediction, but its prediction range is larger than the actual range, which will lead to the waste of fire prevention and control resources and increase the cost. In order to reduce the prediction error, a combination of the Rothermel model and the FCN network identification method is used to synchronize the fire prediction (the prediction is performed as soon as the fire is identified and iterated at a certain frequency). Compared with the independent models, the combined model can effectively reduce the errors caused by individual models to a certain extent, thus improving the accuracy of the overall model.

The remainder of this article is organized as follows. The fundamentals of FCN are described in Section 2, alone with the approach to fire scenario segmentation is described in Section 2. The mathematical derivation and fundamentals of the Rothermel fire spread prediction model are also described in Section 2. Experiments are carried out in section 3 to verify the effectiveness of FCN network, Rothermel model, and FCN-Rothermel synchronized fire identification and prediction for hill fire prevention and control. Section 4 serves as the conclusion.

2. Scene Segmentation of a Fire

2.1. Segmentation Strategy and Architecture

The core idea of Fully Convolutional Network, as a pioneering framework for end-to-end pixel-level semantic segmentation, is to achieve dense prediction of input images of arbitrary sizes through fully convolutionalization with an upsampling mechanism. This experiment is based on the paper "Fully Convolutional Networks for Semantic Segmentation" published by Shelhamer et al. in 2015, and a number of optimizations are carried out on the basis of the original architecture, the structure of which is shown in Figure 1. We replace Backbone from VGG/GoogLeNet to ResNet, adjust the layer structure of feature fusion, and introduce auxiliary classifiers to improve training efficiency and segmentation accuracy. Specifically, the original FCN adopts VGG16 as the feature extractor, and achieves full convolutionalization by removing the fully connected layer and adding 1×1 convolutional and transposed convolutional layers, but the resolution of its deeper features is too low (e.g., the output of the pool5 layer is 1/32 of the original image), which leads to serious loss of details after upsampling. This experiment improves this by first choosing ResNet-50 or ResNet-101 as Backbone, utilizing its residual structure to alleviate the problem of gradient vanishing in the deep network, and constructing a multi-scale feature pyramid by cross-layer jump connection (e.g., merging the outputs of ResNet's layer3, layer4, and layer5 with the up-sampled features, respectively), which significantly improves the segmentation ability of small targets and edge details. In terms of layer adjustment, the original FCN-8s only fused pool3, pool4, and pool5, while this experiment dynamically adjusted the number of jump connections (e.g., increasing the shallow features of layer2 to participate in the fusion) and combined with the adaptive upsampling coefficients, which enabled the network to automatically optimize the feature fusion paths according to the different input resolutions, which demonstrated better performance in recognizing complex scenarios, such as forest fires. This design shows stronger generalization in identifying complex scene datasets such as forest fires.

In addition, this experiment refers to the official implementation of PyTorch and introduces the Auxiliary Classifier in the FCN Head module, which serves to apply additional cross-entropy loss to the intermediate layer features (e.g., layer4 output from ResNet) during the training phase, accelerating the model convergence through the multi-task learning mechanism and enhancing the gradient back propagation effect. In terms of implementation details, the auxiliary classifier consists of 3×3 convolution, batch normalization with ReLU activation function, and its outputs are weighted and fused with the predictions from the main branch by bilinear interpolation up-sampling to the original image size, which ultimately forms an end-to-end trainable architecture. It is worth mentioning that this experiment also optimizes Backbone's pre-training strategy: using ResNet weight initialization pre-trained in ImageNet in conjunction with COCO, instead of the original FCN relying on ImageNet classification pre-training only, which enables the model to better capture the fine-grained features required for semantic segmentation.

Compared with the original FCN, the improved version of this experiment significantly improves the segmentation accuracy and inference efficiency through the deep-feature extraction capability of ResNet, the detail enhancement mechanism of multilevel jump connections, and the regularization of auxiliary classifiers, while maintaining the advantages of full convolutionalization, arbitrary size inputs and end-to-end training.

Figure 1
Framework of the FCN-Based Segmentation Network.

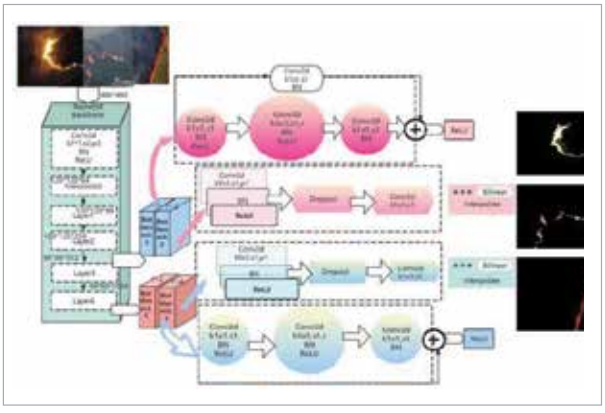

2.2. Backbone: Resnet 50

ResNet50 is a classical deep residual network, and its core idea is to solve the common gradient vanishing and exploding problems in deep neural networks by introducing residual structures, so as to achieve the training and optimization of deeper networks. ResNet50 consists of 50 convolutional layers, and its structure is shown in Figure 2. ResNet50 is divided into five main stages, and each stage contains a different number of residual blocks These residual blocks are classified into two types, Conv Block and Identity Block, Conv Block is used to increase the depth of the network, while Identity Block is used to keep the dimension of the feature map unchanged. In the structure of ResNet50, the first stage consists of a 7x7 convolutional layer and a maximal pooling layer, which is used for the initial extraction of the image features. The second to fifth stages each consist of multiple residual blocks, where the first stage's residual block contains a convolutional layer with a step size of 2, and the rest of the stages have a residual block with a step size of 1, and the number of residual blocks in each stage is 3, 4, 6 and 3, respectively. The residual structure is inspired by the constant mapping, which is formed by adding the inputs directly to the outputs to form a constant mapping, which allows the network to learn a residual mapping between inputs and outputs. The residual mapping between the input and the output, thus avoiding the gradient vanishing problem. The basic form of the residual block is F(X)+X, where F(X) is the feature map processed by the convolutional layer and the activation function, and X is the input feature map.

Figure 2

Layer-wise Configuration of ResNet-50 Network.

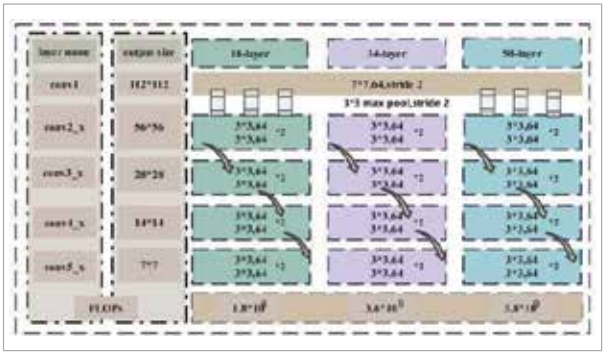

The BN layer in ResNet50 is widely used before each residual block to normalize the input data. The role of the BN layer is to adjust the meaning of the input data to 0 and the variance to 1, thus speeding up the training process and improving the stability of the model. Equation (1) is the formula for the BN layer, where x_i is the original input data, $\hat{x}_i$ and $\hat{y}_i$ is the standardized output data. μ and σ^2 are the mean and variance of the input data, respectively, ε is a small constant to prevent the denominator from being zero, γ and β are learnable parameters.

$$\begin{cases} \mu = \dfrac{1}{m}\sum_{i=1}^{m} x_i \\ \sigma = \dfrac{1}{m}\sum_{i=1}^{m}\left(x_i - \mu\right)^2 . \\ \hat{x}_i = \dfrac{x_i - \mu}{\sqrt{\sigma^2 + \varepsilon}} \\ \hat{y}_i = \gamma \hat{x}_i + \beta \end{cases} \quad (1)$$

ResNet50 adopts the Bottleneck design to reduce the computation and improve the efficiency, the Bottleneck module consists of three convolutional layers, including two 1x1 convolutional layers and one 3x3 convolutional layer, the 1x1 convolutional layer is used for dimensionality reduction or dimensionality upgrading while the 3x3 convolutional layer is used for feature extraction, this design not only reduces the number of references, but also improves the expressive power of the network, the In the structure of Bottleneck module, the first 1x1 convolutional layer reduces the number of input channels from C_in to C_bottleneck, the second 3x3 convolutional layer carries out feature extraction on the downscaled feature maps, and the third 1x1 convolutional layer recovers the feature maps to the original number of channels, C_out. The ReLU activation function is widely used in ResNet50. Equation (2) is the formula for ReLU. The main advantages of ReLU function are computational simplicity and ability to alleviate the problem of gradient vanishing. Its powerful feature extract capability and efficient computational performance show excellent performance in the task of semantic segmentation in dealing with images of fire scene.

$$f(x) = \max(0, x) . \quad (2)$$

Figure 3
Detailed Structure of a Residual Block with Bottleneck.

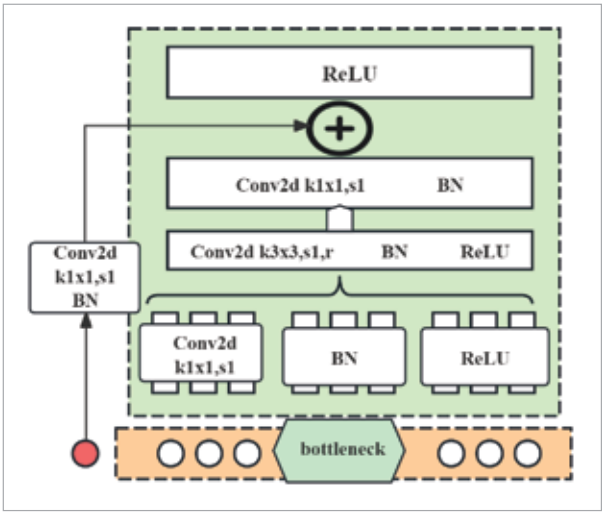

2.3. FCN Head Module

FCN Head module is the key component to realize pixel-level semantic segmentation in the full convolutional network, and its structure mainly includes three parts: feature map dimensionality reduction, bilinear interpolation, and auxiliary classifiers, and its structure is shown in Figure 3. First, the number of channels of the feature map is reduced from a high dimension to the same dimension as the number of categories through a 1x1 convolutional layer. The feature map output from the Backbone of ResNet50 is adjusted to 512 channels after a 3x3 convolutional layer, and then it is adjusted to the number of channels of the categories through a 1x1 convolutional layer. Next, the feature map is restored to the size of the original image using a bilinear interpolation method.

In order to prevent the error gradient from not being passed to the shallow layers of the network, the FCN Head module introduces an auxiliary classifier which usually extracts features from the Layer3 layer of ResNet and is processed in parallel with the main branch. The auxiliary classifier provides additional supervised signals during the training phase, but is removed during the prediction phase. The main functions of the FCN Head module include feature map dimensionality reduction, restoring the original dimensions and auxiliary classifiers. The number of channels of the feature map is adjusted to the number of channels of the category through a 1x1 convolutional layer to achieve the prediction of the classification of each pixel point. The dimensionality reduced feature map is restored to the same dimensions as the input image through the bilinear interpolation method to ensure that the model is able to output the classification results corresponding to the spatial location of the input image. By extracting the features from the deeper layers of the network and classifying them, the auxiliary classifiers can enhance the performance of the model, especially in the training phase (Figure 4).

Figure 4
Schematic Overview of the FCN Head Module.

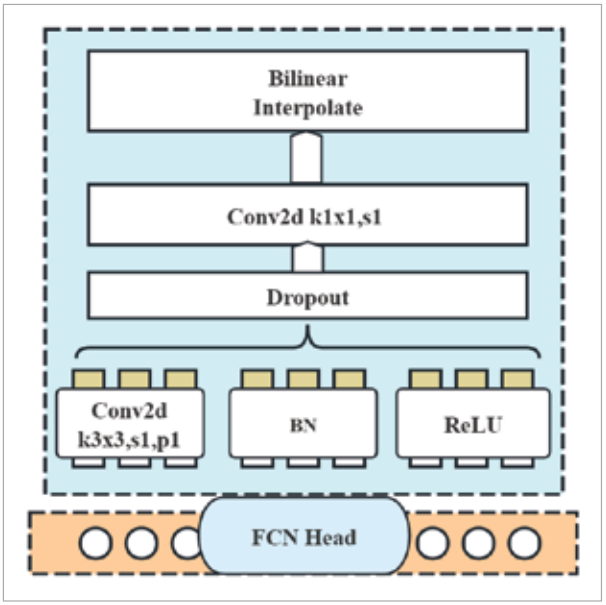

3. Prediction of Fire Spread Trends

Although computer neural network recognition of fire can give the range of fire in time, the study of fire spread is necessary because forest fire is a dynamic process, and the tendency of fire spread will affect the later fire-fighting action and fire rescue. The main work of this study is to select a burning forest, construct the improved Rothermel model for fire spread prediction based on the fire extent obtained by deep learning performed by computer, and verify its performance in simulating fire spread. The

methodology of this research is divided into three parts: data collection and preprocessing, selection of parameters for construction and model validation. This section focuses on the modeling methodology construction and model validation of the proposed improved Rothermel model.

The Rothermel model was proposed by the American forester Rothermel in 1972, which is mainly applied to predict the spread of forest fires, and its output is the rate of fire spread, which corresponds to the linear velocity of the propagation of the fire front (m/s). This semi-empirical model combines theoretical first principles and experimental data into a set of equations that converge with Equation (3).

$$R = \frac{I_R \cdot \zeta}{P_b \cdot \varepsilon \cdot Q_{ig}} \cdot \left(1 + \Phi_w + \Phi_s\right). \tag{3}$$

where, R is the rate of fire spread (IV/min); IR is for the flame zone reaction intensity (Btu/ft2.min); ζ is the rate of spread of the fire (no factor); Φ_w is the wind speed correction factor; Φ_s is the slope correction factor; P_b is the density of the combustible bed (lb/ft3); ε is the effective heat coefficient (no factor); Q_{ig} is the heat of preignition, the amount of heat required to ignite a unit mass of combustible material (Btu/lb).

A fire occurs in a given patch of forest, the time of fire occurrence is almost negligible in relation to the time of forest evolution, and under the condition of no strong winds on flat land. This would indicate that the coefficients of combustible bed density, effective heat coefficient, heat of preignition, intensity of reaction in the flame zone, and rate of spread of the fire, etc., are a fixed number in this forest where the fire occurs. Let it be K1, named as forest fire model coefficient.

$$\begin{cases} K_1 = \dfrac{I_R \cdot \zeta}{P_b \cdot \varepsilon \cdot Q_{ig}} + \sigma \\ R = K_1 \cdot \left(1 + \Phi_w + \Phi_s\right) \end{cases}. \tag{4}$$

The Rothermel model can be simplified to Equation (4). For the wind speed correction factor, it can be analyzed in more detail, which is shown in the below Equation (5).

$$\begin{cases} \Phi_w = CU^B \left(\dfrac{\beta}{\beta_{OP}}\right)^{-E} \\ C = 7.47e^{-0.133\sigma^{0.55}} \\ B = 0.02526\sigma^{0.54} \\ E = 0.715e^{-3.59*10^{-4}\sigma} \end{cases}. \tag{5}$$

For the wind speed correction factor, it will be like Equation (6).

$$\begin{cases} \Phi_w = K_2 \cdot U^B \\ \Phi_s = 5.275\beta^{-0.3}\left(\tan\varphi\right)^2 \\ \Phi_s = K_3\left(\tan\varphi\right)^2 \end{cases}. \tag{6}$$

Combining the specific forms of the wind speed correction factor and the slope correction factor, the Rothermel model can be simplified to Equation (7).

$$\begin{cases} R = K_1\left(1 + K_2U^B + K_3\left(\tan\varphi\right)^2\right) \\ R\left(\theta\right) = K_1\left(1 + K_2\left(U\cos\theta\right)^B \right. \\ \left. + K_3\left(\tan\varphi\right)^2\cos^2\theta\right) \end{cases}. \tag{7}$$

3.1. Scene Segmentation Experiment

1 Dataset processing

In the research of fire detection technology, the public dataset generally lacks fine flame morphology annotation information, which has become a key bottleneck restricting the performance improvement of the model. In order to overcome this limitation, this study systematically constructed a set of dedicated datasets containing 268 high-quality annotated images by integrating multi-source data collection and intelligent annotation technology. In the data collection stage, 144 high-resolution aerial fire images covering forests, factories and other scenes were screened out to fully record the dynamic characteristics of flame propagation under different wind conditions. At the same time, a controlled combustion device was used to generate 124 pieces of laboratory data, including 10 sets of steel wool combustion experiments completed outdoors,

which provided basic samples for flame multi-characteristic analysis. The annotation process adopts a hybrid intelligent strategy: the initial annotation of the target position is based on the LabelImg tool (which meets the requirements of the PASCAL VOC format), and the labeling label is "fire". On this basis, the semi-automatic contour extraction is realized by improving the U-Net network, supplemented by manual verification to ensure the boundary accuracy, and finally the XML format annotation file is generated. The dataset is divided into training set and test set at a ratio of 0.85:0.15, including 227 training sets (including 122 aerial images and 105 laboratory images) and 41 test sets (including 22 aerial images and 19 laboratory images).

The data images used in this study were categorized into two parts: background and flame. As an example image, Figure 5(a) shows the original flame photograph and Figure 5(b) shows the corresponding labeled image. The total number of pixels in a single image is calculated to be 513,000, of which the flame region accounts for 19,689 (about 3.8%) and the background region accounts for 493,311 (about 96.2%), with a ratio of nearly 25:1. This obvious difference in number can easily lead to the model focusing excessively on the background region during training.

Figure 5

Original and labeled images: (a)Photographs of the original flame (b) Labeling images.

(a) (b)

2 Evaluation metrics

In semantic segmentation tasks, in order to evaluate the segmentation effect, metrics such as pixel accuracy (PA), Class Pixel Accurracy (CPA), and Intersection over Union (IoU) are usually used. Among them, PA only focuses on pixel-level classification correctness, while IoU considers both the shape and boundary matching of the segmented region. For example, when the predicted region overlaps with the real region only partially, PA may score high due to most of the pixels being correct, but IoU will be significantly lower due to the lack of overlap, which is more in line with the demand for fine segmentation in practical applications. In addition, in remote sensing segmentation tasks, where the target objects are usually small and have complex boundaries, the IoU can reflect the subtle differences in model performance more sensitively. Equation (8) is the calculation formula of IoU, PA and CPA: (where nij denotes the number of pixels of category i predicted to be called category j, ncls denotes the number of target columns (including background), and ti denotes the total number of pixels of category i in the real case).

$$\begin{cases} IoU = \dfrac{1}{n_{cls}} \sum_i \dfrac{n_{ii}}{t_i + \sum_j n_{ji} - n_{ij}} \\ PA = \dfrac{n_{ii} + n_{jj}}{n_{ii} + n_{jj} + n_{ji} + n_{ij}} \\ CPA = \dfrac{n_{ii}}{n_{ji} + n_{ij}} \end{cases} . \tag{8}$$

3 Experimental results

After 20 epochs of training, the performance of the final model on the test set is quantitatively evaluated by the confusion matrix, in which the intersection and concurrency ratio (IoU) for the key target category "fire" reaches 65.8%, which indicates that the model has a strong capability of recognizing the fire region in complex scenarios. Figures 6(a)-6(b) show the labeled and predicted mask images of Figure 5, respectively, and Figure 7 shows the confusion matrix used to represent Figure 8.

Figure 6

labeled mask image and prediction mask map: (a) Labeled mask image; (b) Model-predicted mask image.

(a) (b)

Figure 7
Confusion matrix for predicting results.

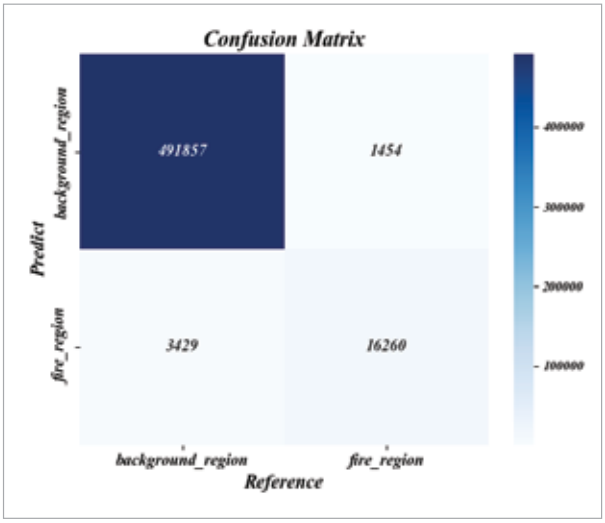

4 Comparison with traditional computer vision methods

Methods based on color features to separate flame regions have significant specificity problems, and the adaptability of different algorithms to flame color varies greatly. Taking the RGB-HIS model as an example, interferences such as green plants and sky can be excluded by setting the red component threshold (R>RT) and the high saturation threshold (ST), but this method is only applicable to flame scenes where the red component is dominant. When processing Image 8(a) (orange flame), the R > G > B rule of the RGB model leads to misjudgment. Similarly, although the YCbCr model reduces light interference by separating luminance (Y) and chromaticity (Cb/Cr), it does not take into account the dynamic relationship between luminance and flame color and will misjudge the highlighted areas as flames in reflective scenes. The HSV model, on the other hand, has a recognition accuracy of more than 90% at the maximum value and 0% at the minimum value in 144 test maps through the joint thresholds of hue ($0 \leq H \leq 0.35$), saturation ($0.3 \leq S \leq 1$) and luminance ($0.8 \leq V \leq 1$), which is a great difference.

Figure 8
Flame color under different conditions: (a) Different colors of flame-yellowish flame; (b) Different Color Flame-Reddish Flame; (c) The effect of cloudy skies on flame color; (d) Flaming area with a lot of smoke.

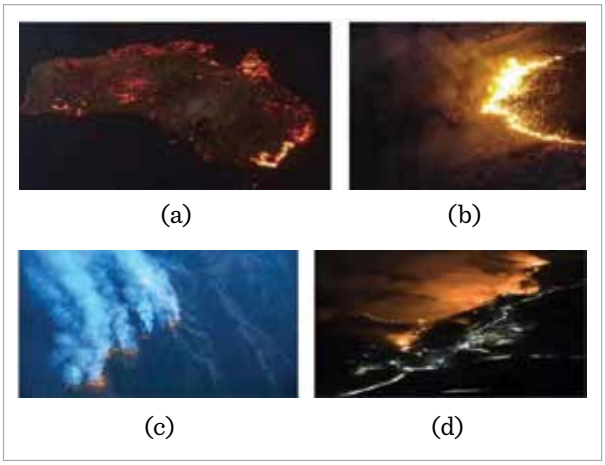

3.2. Fire Prediction Experiment Part

1 The Los Palisades Mountain Fire Experiment

Previously, this paper introduced the Rothermel Forest Fire Spread Prediction Model and made some amendments to it in specific cases to make it more consistent with the prediction needs of forest fire spread in specific cases and to improve the prediction accuracy. The improvement of prediction accuracy not only helps to protect the forest biological and environmental resources in a timely manner, but also effectively reduces the loss of the fire department and the public property. In January 2025, a forest fire occurred in Los Angeles County, California, U.S., causing severe damage. In this paper, the Palisades Fire in Los Angeles County was selected as the research object, and the satellite images of the fire were acquired from NASAfirms website for six days from January 7 to January 12. In order to better validate the Rothermel Forest Fire Spread Prediction Model, it was introduced to predict the trend of the fire spread on each day, and the loss rate was calculated by comparing with the real area of the fire in the next day.

As can be seen from the Figure 9 above, the fire was detected starting on January 7. On January 8, the fire began to spread in a westerly and easterly direction. On January 9, the fire spread rapidly with the effect of Santa Ana winds, and the area of over-fire exceeded the area of the previous day by a factor of more than 30. From January 10 to January 12, the fire spread north of the point of ignition. On January 12, the fire reached its approximate maximum size.

Figure 9
Palisades Mountain Fire spread timeline (Jan. 7-Jan. 12).

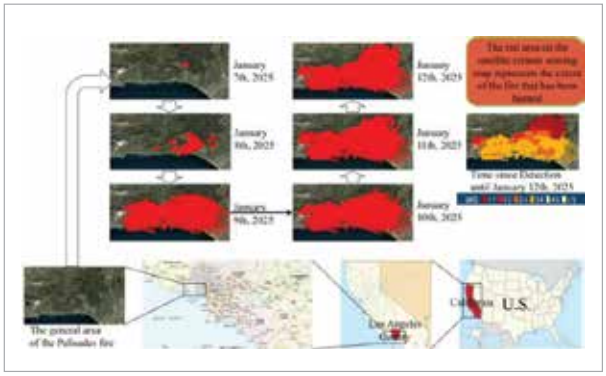

Through the satellite images on January 7, this paper selects "The Summit" location (latitude and longitude: 34.075 N, -118.547 W) as the ignition point, and introduce the Rothermel model to predict the future course of fires in the region.

On January 7, The Summit location was the first to detect the point of origin of the fire. Assuming first that there was no wind in the area at the beginning, the combustible density, effective heat coefficient, and forest fire spread coefficients for the area were combined and substituted into Rothermel's formula to obtain the predicted over-fire area on January 8 (before January 9), which was then compared to the true over-fire area to calculate the loss ratio.

On January 8, the predicted overfire area used The Summit location as the upper focal point, and its predicted overfire area shape approximated an ellipse. Predictions are made based on the new true overfire area, with the constraints of wind speed and land and sea geomorphology, and constraints are added to the model for prediction (Figure 10).

Figure 10
Comparison images of predicted overfire area and actual overfire area from January 7th to January 8th.

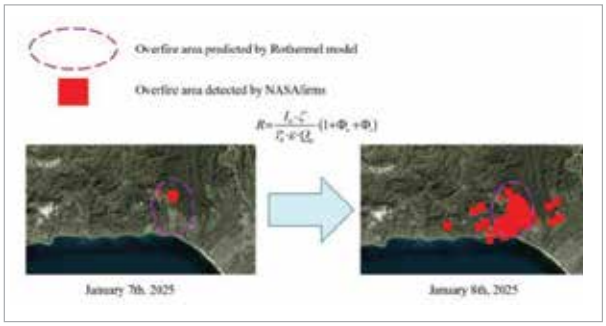

Figure 11
Comparison images of predicted overfire area and actual overfire area from January 8th to January 9th.

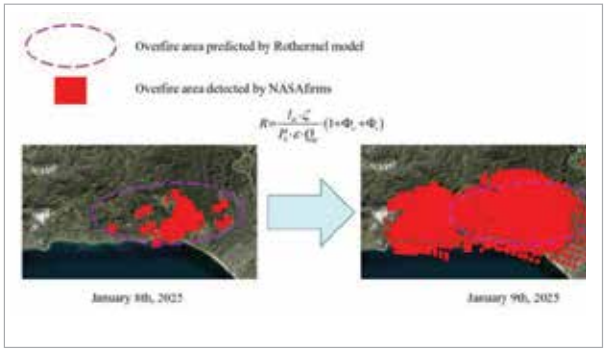

Under the influence of Santa Ana winds, the overfire area spread at an alarming rate from January 8 to January 9, with the overfire area on January 9 reaching nearly 30 times the size of the overfire area on January 8 (Figure 11).

Figure 12
Comparison images of predicted overfire area and actual overfire area from January 9th to January 10th.

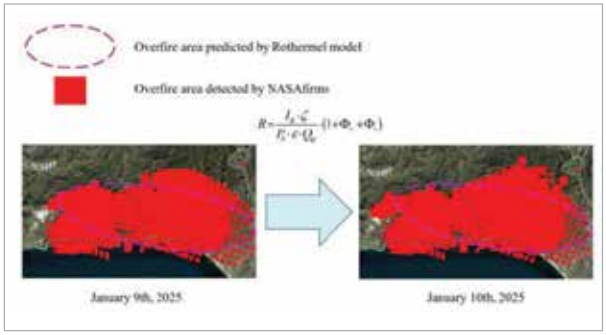

On January 9, the forest fires maintained a predominantly east-west direction of spread, with the southern portion of their overfire area reaching Santa Monica Beach, which has caused property damage in a large residential community. From January 9 to January 10, the east-west spread of the fires remained essentially stationary, and a northward trend in the spread of the forest fires was detected (Figure 12).

On January 10, as some of the fires spread to residential neighborhoods, which have different fire conditions than forests, a categorization discussion was

Figure 13
Comparison images of predicted overfire area and actual overfire area from January 10th to January 11th.

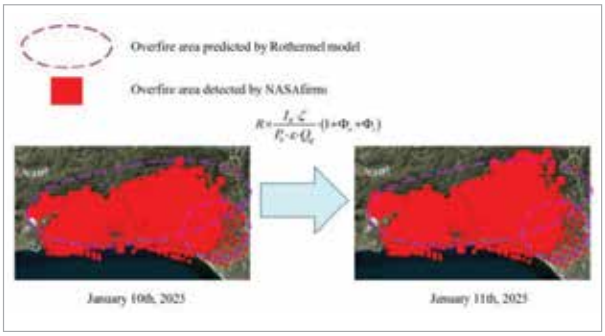

required. Based on the original overfire area, the fire spread trend to the north was still predicted by the original Rothermel forest fire spread model, while the southeast corner of the overfire range (residential communities) was parameterized to better improve prediction accuracy. The improved Rothermel forest fire spread model predicted a nearly circular fire area. Between January 10 and January 11, the fire's spread slowed (Figure 13).

Figure 14
Comparison images of predicted overfire area and actual overfire area from January 11th to January 12th.

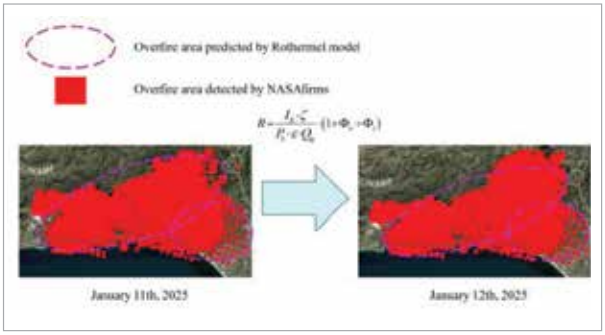

East-west fire spread largely ceased from January 11 to January 12, a day when fires spread primarily in a northerly direction. By January 12, the area over which forest fires had burned was largely fixed (Figure 14).

2 Experimental error analysis

Jorge et al. proposed that the symmetric difference between the predicted fire area and the real fire area based on the corresponding predicted fire area, i.e., the error between the predicted fire area value and the real fire overfire area value for the Rothermel model[33]. Let the predicted fire region be region A and the real fire region be region B. The symmetric difference AΔB corresponds to the concatenation of the two sets minus their intersection, as shown in Equation (9).

$$A\Delta B = \left(A \cup B\right) - \left(A \cap B\right). \tag{9}$$

In order to reduce the systematic error of poor symmetry caused by insufficiently fine area identification (including fire identification area and predicted spread area), this paper adopts the closed curve integral for the area of these areas to improve the height of area identification. Martin et al. proposed the Green's formula integral for the area of time area [5]. And since the Rothermel model in this paper predicts curves that are approximately elliptical rather than perfectly elliptical nonsmoothed curves, the integral formula has to be improved, and Claf et al. [9] in referring to celestial motions that are approximately elliptical orbits propose the multi-point discretization of elliptical orbits of planetary bodies, and abstract it to orbits resulting from the summation of the limits of the discretized points. For this, Ananthan and Gaurav [2] then used the Gaussian area formula (shoestring formula) of the discretization method to solve for the area of the graphical region whose boundary consists of discrete points.

$$A = \iint dA = \frac{1}{2}\oint \left(xdy - ydx\right). \tag{10}$$

$$A = \left|\sum_{i=1}^{n}\left(x_i y_{i+1} - x_{i+1} y_i\right)\right|. \tag{11}$$

Equation (10) is the Green's formula, in order to avoid the calculation accuracy failure caused by the non-smooth curve, this paper adopts the shoelace formula (11) on the basis of the Green's formula to solve the simulated fire area A and the real fire area B, and arrives at a more suitable method by comparing the two types of calculation methods.

At the same time, these fire regions are divided into a finite number of square raster's of the same size and

ensure that the size of the number of raster's is larger than 10000 to improve the accuracy for the fitness function solution. Since both the results of the fire spread simulation and the actual prescribed fire data consist of corresponding burning mini-raster's, the fitness function is given by the following equation in order to calculate the symmetric difference between the two groups and to assess the quality of the candidate solution Si:

$$RSD_i = \frac{(A \cup B)_{grid_i} - (A \cap B)_{grid_i}}{R_{grid_i} - I_{gird_i}}. \quad (12)$$

$Ugrid_i$ Corresponds to the number of rasters in the two concatenated sets $\bigcap grid_i$ corresponding to the number of rasters in the intersection of the two sets. R_{grid_i} is the number of grids actually burned. I_{grid_i} is the number of grids actually lit. R_{grid_i}-I_{grid_i} is due to the fact that the fitness is calculated using the number of grids actually burned, i.e., it is the relative error of the fitness function. The fitness function also represents the stability of the model to some extent. The fitness function of the area of the region obtained by solving the two integration methods is used to assess the model stability RSDi.

After algorithmic solution calculations, this study produced the symmetry difference AΔB of the predictive model for the Los Angeles Palisades Hill Fire from January 7 to January 12, the predicted area values obtained from the two methods (integral vs. infinite series) of solution, and the model fitness function RSDi, as shown in the following figure.

Figure 15

Palisades Mountain Fire Prediction Error and Evaluation Metrics.

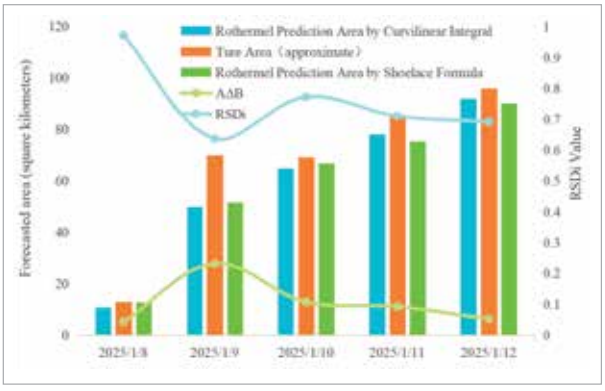

As can be seen from Figure 15, the predicted area values obtained by the two calculation methods do not differ much, and in general, the total error of the shoelace formula method is relatively small. However, it is worth mentioning that the accurate predicted values of the shoelace formula method have a larger error in the later stages of fire spread, and the accurate predicted values of the curve integral method have a larger error in the early stages of fire spread. This is related to the burning out of combustibles in the later stages of the fire. The symmetry difference shows a trend of increasing and then decreasing, and the symmetry difference is the largest on January 8, and the decrease of symmetry difference in the later stage shows that the model has accuracy but also has a certain lag. The fitness function RSDi shows a decreasing and then increasing trend, and finally tends to equilibrium (0.7), indicating that the prediction results of the Rothermel prediction model are acceptable. Overall, the prediction of the Palisades Hill Fire in Los Angeles proves the applicability of the Rothermel model, but there are certain errors and backwardness of the technology of confirming the predicted area, and the change of the experimental environment that exists during the spread of the fire leads to the deterioration of the stability of the Rothermel model in the middle stage of the experiment, which requires manual intervention and increases the experimental error and experimental cost. In the middle stage of fire spread, it is recommended to use manual intervention or multiple hybrid modeling methods to reduce the experimental error.

3.3. Comprehensive Experiment

This study focuses on the coupling mechanism between FCN network and Rothermel model and its synergistic effect in fire dynamics prediction. In the framework of the integrated experiment, FCN serves as the core module of fire field identification, and its output binary mask directly determines the initial fire field boundary of the Rothermel model. Although FCN has achieved 65.8% IoU in the prelude test, edge blurring or local omissions (e.g., smoke obscured areas) in its segmentation results will directly affect the input accuracy of the Rothermel model: for example, if FCN misclassifies a portion of the fire boundary as an unburned area, the Rothermel model will underestimate the spreading potential of the direction due to the absence of the initial fireline,

resulting in the contraction of the predicted contour to the west. This error conduction is nonlinear in nature-fire shape deviations not only change the local spread direction, but also trigger global prediction shifts through fire interactions (e.g., flame merging). To mitigate this problem, the experiment introduces morphological post-processing at the data interface layer, which performs expansion and smoothing operations on the discretized boundaries of FCN outputs to repair small holes and fill in broken edges, thus enhancing the continuity of the initial fire line and reducing the sensitivity of the Rothermel model to segmentation noise. This optimization mechanism makes the combination between FCN and Rothermel smoother and significantly improves the prediction robustness in complex environments.

1 Experimental scene

The experimental site was constructed in a controlled open-air environment with a mixture of leaves, dead grass and low shrubs to simulate the structure of typical mountain surface combustibles. The size of the combustion bed was 2m×2m (total area of 4m^2), and the thickness was strictly controlled at 5cm to ensure the uniform distribution of fuel through layered compaction. The vegetation ratios refer to the common combinations of dead combustibles on the forest surface, with about 30% of dead branches, 40% of dry fallen leaves, and 30% of shrub residues, in order to restore the fuel heterogeneity of a real fire. The experiments were chosen to be conducted at night to improve the accuracy of the visual recognition system by utilizing the high contrast properties of the flames and the dark background. Under windless conditions (wind speed <0.2 m/s), environmental parameters, including air temperature (4.4±1.0°C), relative humidity (45±5%), etc., were continuously monitored at the same time. The ignition device adopts the resistance wire ignition method, and the initial ignition source is placed at the center of the combustion bed.

2 Flame area identification

In this experiment, four typical time nodes were selected based on the flame area growth rate and motion characteristics: T1 (early fire initiation, flame area share <5%), T2 (diffusion acceleration period, area share 15%-20%), T3 (stable combustion period, area share 30%-35%), and T4 (recession period, area share 25%-30%).

T1 stage (IoU=35%): The flame region in this stage is characterized by dispersed star fire points with blurred edges and obvious dynamic flickering. Traditional edge detection methods (e.g., Canny operator) often cause contour breakage due to noise interference in this stage, while FCN can reduce the noise sensitivity through deep feature learning, but it is still difficult to localize tiny targets (<50 pixels).

T2-T3 stage (IoU=64%-71%): As the fire intensifies, the flame region forms a continuous thermal radiation belt with significant edge gradient features. At this time, the feature extraction advantages of FCN are fully realized: the ResNet-50 pre-trained model can effectively capture the high-frequency texture features of the flame (e.g., turbulent fluctuation patterns).

Stage T4 (IoU = 69%): Although the total flame area decreases, the residual radiation from the high temperature products maintains a strong edge contrast. The decrease in IoU at this point mainly stems from the semantic segmentation confusion between the flame core area and the non-uniform residual flame area.

3 Fire spread prediction

In Section 4.3.1. this paper carries out an identification experiment for T1-T4 stage flames, based on this fire experiment and the Rothermel fire spread model, this paper predicts the overfire area as well as the spreading tendency at the end of the i(1-4) stage to the end of the i+1(2-5) stage and gives the approximate predicted range of overfire area.

Stage T1 (small variation coefficient of curvature of the spreading area curve): the flame area in this stage is concentrated and of circular shape, and based on its contour and fixed experimental parameters, it is concluded that the predicted overfire area of Stage T2 is about 0.915 square meters, and at the same time, it is also concluded that the approximate spreading direction of the fire is in the direction of 8.0° north by east.

Stage T2 (spread area curve curvature change coefficient began to increase): this stage of the flame area began to predict the direction of the left deviation 34.9° direction of the spread (i.e., the direction of 26.9° north of west), and this direction and its opposite direction for the ellipse of the long axis (approximate ellipse) to spread, resulting in T3 stage of the predicted area of the fire area of about 1.591 square meters.

Stage T3 (the curvature variation coefficient of the spreading area curve begins to decrease): In this stage, the flame area begins to spread in the direction of 31.4° to the right of the predicted direction (i.e., in the direction of 4.5° to the east of the north), and results in the predicted over-fire area of about 2.228 square meters in Stage T4. At the same time, the main body of the flame no longer spreads in the predicted direction, but spreads in all directions at a microscopic angle (gradually evolving from an irregular shape to a circle-like shape, with the coefficient of variation of curvature starting to decrease).

Stage T4 (Spread Area Divided into Two Parts): In this stage, the fire area changes to two irregular shapes as the combustible material in the center area of the fire burns out and the flame area breaks into two parts. Similar to the Los Palisades Hill Fire, when the fire spreads to a certain extent, the fire area changes into two or more unconnected areas. In the microcosm, the area of burned-out combustible material cannot be recognized in the Rothermel model, which leads to the prediction error of the Rothermel model will be large. Finally, the predicted overfire area of the T5 stage is about 3.106 square meters.

Unlike the fire spread predictions for the Palisades Mountain Fire in Los Angeles, the Rothermel model has a smaller prediction error under macro conditions, but the relative error of the Rothermel model is smaller under the micro conditions of small, simulated fires. Also, in the later stages of fire spread (T4 and later stages), the Rothermel model can be divided into multiple parts for prediction in large fires, but it is difficult to divide into multiple parts for prediction in small fires. In conclusion, the Rothermel prediction model is more applicable in large fires, but in small fires, the Rothermel model has a higher prediction accuracy (only for the first and middle stages of fire spread).

Figure 16

Comprehensive experimental comparative analysis chart.

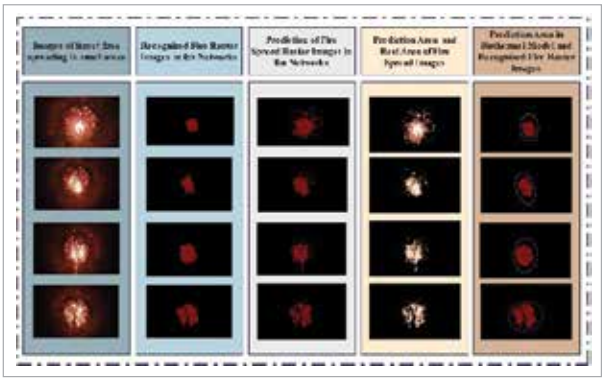

4 Comprehensive experimental error

By comparing the errors of four consecutive moments, the initial recognition errors of FCN neural network are 60%, 36%, 29%, and 31%, while the prediction errors corrected by Rothermel model are significantly reduced to 30%, 7.2%, 4.95%, and 7.05%. Figure 16 shows the FCN recognition error versus the prediction error corrected by the Rothermel model.

Figure 17

Comparison of Rothermel prediction error and FCN identification error.

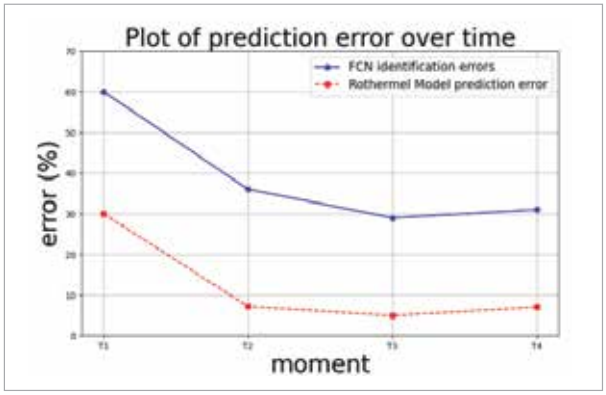

Rapid convergence of initial moment error: the recognition error of FCN in the first moment is as high as 60%, but the error drops by 50% directly after Rothermel correction, which indicates that the physical model has strong correction ability for initial misjudgment. This correction stems from Rothermel's physical constraints on the direction and speed of fire spread, such as dynamically adjusting the position of the fire line through the reaction strength parameter (Figure 17).

Stability of the mid-term error: the error between the second and third moments is reduced from 36% to 4.95%, an error reduction of more than 85%. This reflects the continuous adaptability of the Rothermel model to dynamic fires, e.g., through real-time feedback of fuel load, wind speed, and terrain parameters, which suppresses the accumulation of errors in the FCN due to image noise or occlusion.

Slight rebound in the terminal error: the slight increase in the error to 7.05% at the fourth moment may be related to the complexity of environmental factors (e.g., sudden changes in wind direction, changes in fuel moisture) in the later stages of fire spread. However, the overall error is still significantly lower than the pure FCN model, indicating that the joint model has the ability to resist interference.

5 Comprehensive experimental results analysis

In order to better quantify the predictive effectiveness of two prediction experiments, the Rothermel model prediction of Palisades fires and the Rothermel model prediction of fires with the addition of the FCN fire recognition network corrected for fire area, this paper uses two composite error tables (Tables 1-2) to show the improvement in the accuracy of the Rothermel model prediction with the addition of the FCN fire recognition network corrected for fire area and methods to improve the accuracy improvement within the Rothermel prediction model. accuracy improvement, and methods to improve the accuracy improvement within the Rothermel prediction model.

Table 1
Error of Rothermel Prediction Model by two approximation method.

	Accuracy Improvement by Curvilinear Integral			
	Date	Prediction area	Real area	AΔB
Accuracy of Experiment on the Rothermel Model's Prediction of the Palisades Fire	Jan. 8th	10.891	12.901	5.172
	Jan. 9th	49.913	69.917	27.814
	Jan. 10th	64.874	79.316	12.919
	Jan. 11th	78.196	84.891	11.119
	Jan. 12th	92.137	95.901	6.318
	Accuracy Improvement by Shoelace Formula			
	Date	Prediction	Real	RSDi
	Jan. 8th	12.741	14.901	0.971
	Jan. 9th	51.573	67.462	0.637
	Jan. 10th	66.874	78.316	0.772
	Jan. 11th	75.389	86.194	0.71
	Jan. 12th	90.137	94.754	0.691

Table 2
The accuracy of FCN-RotTaTable 2 The accuracy of FCN-Rothermel Comprehensive Experiment Compared to Traditional Rothermel Model.

Analysis of FCN-Rothermel Comprehensive Experiment				
T1	FCN-Rothermel prediction area	0.915	Original prediction accuracy	0.844
	Real fire area	0.871	Prediction accuracy with FCN	0.952
T2	FCN-Rothermel prediction area	1.501	Original prediction accuracy	0.713
	Real fire area	1.486	Prediction accuracy with FCN	0.989
T3	FCN-Rothermel prediction area	1.778	Original prediction accuracy	0.818
	Real fire area	1.674	Prediction accuracy with FCN	0.942
T4	FCN-Rothermel prediction area	2.506	Original prediction accuracy	0.921
	Real fire area	2.397	Prediction accuracy with FCN	0.956

Note: The data represented in Tables 1-2 were not derived in the same experiment. All data units in Table 1 are per square kilometer and all data units in Table 2 are per square meter. Through different approximation methods, the true overfire area of the two also differ, but the error from the true value did not exceed 2%-3%. Each prediction value in Table 2 is the mean of the predictions from multiple experiments in a specific stage (excluding outliers), as a way to reduce the error in a single experiment. Original prediction accuracy is the accuracy of the fire area predicted by the original Rothermel model alone without the FCN. Original prediction accuracy is derived from the experimental results in Table 1.

Equations (10)-(11) give two more accurate approximation methods for the Rothermel model to predict the fire area (the traditional curve integral method and the shoelace formula method). AΔB and RSDi indicate the stability and accuracy of the two approximation methods, respectively. The values of AΔB and RSDi in Table 1 indicate that these two approximation methods are excellent performers in this experiment, but these two approximation methods cannot be compared in terms of accuracy by these two measures because these two measures cannot be compared directly.According to Table 1, if the comparison is made based on the results of the difference between the true fire area and the predicted fire area only, then it can be seen that the shoelace formula approximation method to improve the prediction accuracy of the Rothermel model is better than the traditional curve integral approximation method.

It can also be concluded that the prediction accuracy of the Rothermel model is improved after adding the FCN fire recognition network to correct the fire area. The prediction accuracy with FCN is 5% to 20% higher than that without FCN in the same case. This indicates that the accuracy of the traditional prediction model is effectively improved by adding the correction of the deep learning neural network model. This suggests that the combined model attempted in this paper is advantageous when compared with existing methods as verified by comprehensive experiments.

The Rothermel model not only corrects the initial identification bias of the FCN, but also continuously optimizes the prediction trajectory through physical rules (e.g., differential equations for fire propagation), so that the error shows a tendency to converge rather than diverge. There are four possible reasons why the Rothermel composite FCN is so effective, specifically:

The Rothermel model combines physical principles with data-driven approaches, leveraging heat transfer and fuel reaction strength formulas verified by laboratory data to describe fire propagation laws accurately. Meanwhile, the FCN captures spatial fire zone characteristics through extensive image data learning. This integration allows physical constraints to correct data when FCN misjudges due to image blurring or smoke interference, adjusting fire boundaries via propagation velocity formulas and shifting recognition areas toward real fire zones[30]. For instance, the MD-CA model reduces area error rates to 9.42%-15.63%[32], outperforming traditional CA models. Additionally, Rothermel's parameters like wind speed and slope are dynamically optimized using genetic algorithms or real-time meteorological data, compensating for FCN's rigidity caused by static training data [14].

The model suppresses error propagation by addressing FCN's initial segmentation biases, such as confusing flames with smoke. Rothermel prioritizes correcting anomalous fire area predictions inconsistent with wind direction and terrain slope using an eight-direction velocity formula. Terrain slope alone can double fire spread speed. FCN struggles to extract from images [22]. Furthermore, Rothermel estimates combustion intensity via fuel sample data, recalculating fire-line positions through weighted averaging when FCN's identified regions mismatch fuel distribution. This prevents stepwise error amplification while maintaining alignment with physical conditions.

Rothermel and FCN co-optimize time series forecasting by preserving historical states: FCN retains fire zone textures through convolutional layers, while Rothermel tracks temporal dynamics via fire propagation differential equations. Their synergy resembles an LSTM model that captures both spatial and temporal dependencies. Predictions are iteratively refined as Rothermel's outputs at each timestep serve as prior inputs for FCN in the next step, forming a closed-loop system. For example, multi-core CNNs enhance accuracy through multi-

scale feature fusion, while Rothermel's physical rules sharpen sensitivity to fire line edges [22].

Robustness is strengthened through multi-source data fusion, integrating non-visual inputs like meteorology, terrain, and fuel properties with FCN's image-based features. This approach ensures stability in complex environments—such as haze or glare interfering with images—by relying on wind speed and humidity parameters. Additionally, Rothermel compensates for FCN's limited regional generalization using empirical formulas like Byram's Fireline intensity equation, adapting to area-specific conditions while maintaining predictive reliability across diverse forest landscapes [8, 27].

6 Ablation experiment

In the design of ablation experiments, we systematically isolate and reorganize the core method modules to quantitatively evaluate the contribution of each component to the prediction of fire spread by using the principles of modular decomposition and incremental validation. A three-layer verification system was constructed: firstly, the widely used Faster RCNN was used as the traditional baseline model; Secondly, independently verify the performance of a single module - Finally, the joint strategy is verified by the cascade fusion architecture, and the probability graph of the live line output by the FCN is used as the initial boundary condition of Rothermal, and a two-way feedback mechanism is established to make the propagation heat flux calculated by the physical model feed back to the FCN feature decoder in real time. In order to objectively quantify the performance, the spatiotemporal error separation measurement method was used to calculate the coincidence error of the spread area at the four key time nodes of fire evolution (T1 fire period, T2 accelerated spread period, T3 stable combustion period, and T4 attenuation period), and the consistency of data homology, computing resources and physical parameters was strictly controlled.

In this study, the performance of different fire spread prediction methods was evaluated through systematic comparative experiments. As shown in Table 3, the prediction error rates of the traditional Faster RCNN method are 41%, 37%, 31%, and 35% on four consecutive time nodes (T1-T4), respectively. In contrast, in the single model prediction, the error rate of the Rothermel physical model is maintained

Table 3
Comparison of ablation experimental errors.

	Faster-rcnn (Traditional Method)	Rothermel	FCN-Net	Rothermel +FCN
T1	41%	39%	60%	30%
T2	37%	37%	36%	7.3%
T3	31%	31%	29%	4.9%
T4	35%	33%	31%	7.0%

in the range of 31%-39% at T1-T4. The error of the FCN neural network is as high as 60% at T1, but it is significantly improved to 29%-36% at T2-T4. It is worth noting that the joint forecasting method of Rothermel and FCN shows significant advantages: the error rate is reduced to 30% at T1, 7.3% at T2, 4.9% at T3, and 7.0% at T4. The error rate of this joint method at T2-T4 is 76%-83% lower than that of the optimal single model (e.g., 4.9% at T3 versus 29% lowest for single model). The experimental results clearly show that the joint prediction method has a continuous accuracy advantage. Especially in the middle and late stages of fire propagation (T2-T4 stage), the error rate of the combined method is always stable below 7.3%, which is significantly lower than that of the FCN single model (29%-36%) and the Rothermal single model (31%-37%).

4. Conclusion

Aiming at the social pain points of ecological degradation and multiple types of property losses caused by the spread of hill fires, this paper utilizes hill fire recognition and prediction techniques to conduct comparative study with a combination of micro-macro perspectives. Based on the traditional fire recognition technology, this paper improves the model to obtain Fully Convolutional Network (FCN), which adapts to the recognition of multiple flame colors and shows good robustness compared with the traditional model. Based on the Rothermel model of fire spread, this paper improves the model and uses the Palisades fire in Los Angeles as a case study for prediction, and the model is verified to have high accuracy in prediction through error analysis. After confirming the applicability and

combinability of the two types of models, this paper conducts experiments by simulating a microscopic mountain fire environment, and applies the Rothermel model for fire spread prediction based on the FCN for fire identification, and establishes a multi-stage research on the prediction and prevention of fires from the start of the fire to the spread and the end of the fire. The study analyzes the recognition and prediction accuracy of the combined FCN-Rothermel recognition-prediction model through the four stages of fire spread and finds that the respective shortcomings of the FCN and Rothermel models can be complemented. For example, in the T3 stage of fire propagation, when the initial combustible material is burned out and the area of the burning place is reduced, the Rothermel model cannot identify the experimental error, and the FCN model can identify the burned out area and realize the reduction of prediction error. Finally, the experimental error analysis in this paper shows that the FCN-Rothermel identification-prediction combination model fits well, effectively reduces the experimental error of the traditional modeling method, improves the identification and prediction efficiency, and to a certain extent provides an innovative point and a new way of thinking for the identification and prevention of hill fires. However, there are still flaws in this model, and the ability of the combined model to adapt to changes in different environments needs to be further studied.

Data Availability Statement

The datasets used and/or analyzed during the current study are available from the corresponding author on reasonable request.

Conflicts of Interest

The author(s) declared no potential conflicts of interest with respect to the research, author-ship, and/or publication of this article.

Funding

The author(s) received no financial support for the research, authorship, and/or publication of this article.

References

1. Abdusalomov, A. B., Islam, B. M. D. S., Nasimov, R., Mukhiddinov, M., Whangbo, T. K. An Improved Forest Fire Detection Method Based on the Detectron2 Model and a Deep Learning Approach. Sensors, 2023, 23(3), 1512. https://doi.org/10.3390/s23031512
2. Ananthan, M., Gaurav, T. Interface Reconstruction and Advection Schemes for Volume of Fluid Method in Axisymmetric Coordinates. Journal of Computational Physics, 2021, 446, 110663. https://doi.org/10.1016/j.jcp.2021.110663
3. Appana, D. K., Islam, R., Khan, S. A., Kim, J. M. A Video-Based Smoke Detection Using Smoke Flow Pattern and Spatial-Temporal Energy Analyses for Alarm Systems. Information Sciences, 2017, 418, 91-101. https://doi.org/10.1016/j.ins.2017.08.001
4. Barmpoutis, P., Papaioannou, P., Dimitropoulos, K., Grammalidis, N. A Review on Early Forest Fire Detection Systems Using Optical Remote Sensing. Sensors, 2020, 20(22), 6442. https://doi.org/10.3390/s20226442
5. Bohner, M., Guseinov, G. S. Line Integrals and Green's Formula on Time Scales. Journal of Mathematical Analysis and Applications, 2007, 1124-1141. https://doi.org/10.1016/j.jmaa.2006.03.040
6. Buryak, L. V., Kukavskaya, E. A., Ivanov, V. A., Malykh, O. F., Kotelnikov, R. V. Assessment of Fire Hazard and Its Dynamics in Forest Areas of Siberia. Contemporary Problems of Ecology, 2021, 14, 803-814. https://doi.org/10.1134/S1995425521070040
7. Byari, M., Bernoussi, A., Jellouli, O., Ouardouz, M., Amharref, M. Multi-Scale 3D Cellular Automata Modeling: Application to Wildland Fire Spread. Chaos, Solitons & Fractals, 2022, 164, 112653. https://doi.org/10.1016/j.chaos.2022.112653
8. Calp, M. H., Kose, U. Estimation of Burned Areas in Forest Fires Using Artificial Neural Networks. Ingeniería Solidaria, 2020, 16(3), 1-22. https://doi.org/10.16925/2357-6014.2020.03.08
9. Carl, F., Craver, M. P. The Directionality of Distinctively Mathematical Explanations. Studies in History and Philosophy of Science, 2017, 31-38. https://doi.org/10.1016/j.shpsa.2017.04.005
10. Díaz-Avalos, C., Juan, P., Serra-Saurina, L. Modeling Fire Size of Wildfires in Castellon (Spain), Using Spa-

tiotemporal Marked Point Processes. Forest Ecology and Management, 2016, 381, 360-369. https://doi.org/10.1016/j.foreco.2016.09.013

11. Encinas, L. H., White, S. H., Del Rey, A. M., Sanchez, G. R. Modelling Forest Fire Spread Using Hexagonal Cellular Automata. Applied Mathematical Modelling, 2007, 31(6), 1213-1227. https://doi.org/10.1016/j.apm.2006.04.001
12. Fraga, E., Cortés, A., Margalef, T., Hernández, P., Carrillo, C. Cloud-Based Urgent Computing for Forest Fire Spread Prediction. Environmental Modelling & Software, 2024, 177, 106057. https://doi.org/10.1016/j.envsoft.2024.106057
13. Glasa, J., Halada, L. A Note on Mathematical Modelling of Elliptical Fire Propagation. Computing and Informatics, 2011, 30(6), 1303-1319. https://doi.org/10.1111/j.1467-8640.2011.00406.x
14. Hackett, C., de Andrade Moral, R., Mishra, G., McCarthy, T., Markham, C. An Efficient Method to Simulate Wildfire Propagation Using Irregular Grids. Natural Hazards and Earth System Sciences Discussions, 2024, 2024, 1-29. https://doi.org/10.5194/nhess-2024-27
15. Huot, F., Hu, R. L., Goyal, N., Sankar, T., Ihme, M., Chen, Y. F. Next Day Wildfire Spread: A Machine Learning Dataset to Predict Wildfire Spreading from Remote-Sensing Data. IEEE Transactions on Geoscience and Remote Sensing, 2022, 60, 1-13. https://doi.org/10.1109/TGRS.2022.3192974
16. Jing, X., Zhang, D., Li, X., Zhang, W., Zhang, Z. Prediction of Forest Fire Occurrence in Southwestern China. Forests, 2023, 14(9), 1797. https://doi.org/10.3390/f14091797
17. Khennou, F., Akhloufi, M. A. Improving Wildland Fire Spread Prediction Using Deep U-Nets. Science of Remote Sensing, 2023, 8, 100-101. https://doi.org/10.1016/j.srs.2023.100101
18. Kuznetsov, G., Kondakov, A., Zhdanova, A. Mathematical Modeling of Forest Fire Containment Using a Wet Line Ahead of the Combustion Front. Fire, 2023, 6(4), 136. https://doi.org/10.3390/fire6040136
19. Li, F., Zhang, X., Kondragunta, S. Highly Anomalous Fire Emissions from the 2019-2020 Australian Bushfires. Environmental Research Communications, 2021, 3(10), 105005. https://doi.org/10.1088/2515-7620/ac2e6f
20. Liang, H., Zheng, C., Liu, X., Tian, Y., Zhang, J., Cui, W. Super-Resolution Reconstruction of Remote Sensing Data Based on Multiple Satellite Sources for Forest Fire Smoke Segmentation. Remote Sensing, 2023, 15(17), 4180. https://doi.org/10.3390/rs15174180
21. Li, Y., Zhang, W., Liu, Y., Jin, Y. A Visualized Fire Detection Method Based on Convolutional Neural Network Beyond Anchor. Applied Intelligence, 2022, 52(11), 13280-13295. https://doi.org/10.1007/s10489-022-03243-7
22. Marjani, M., Mesgari, M. S. The Large-Scale Wildfire Spread Prediction Using a Multi-Kernel Convolutional Neural Network. ISPRS Annals of the Photogrammetry, Remote Sensing and Spatial Information Sciences, 2023, 10, 483-488. https://doi.org/10.5194/isprs-annals-X-4-W1-2022-483-2023
23. Marziliano, P. A., Lombardi, F., Cataldo, M. F., Mercuri, M., Papandrea, S. F., Manti, L. M., Bagnato, S., Ali, G., Fusaro, P., Pantano, P. S., Scuro, C. Forest Fires: Silvicultural Prevention and Mathematical Models for Predicting Fire Propagation in Southern Italy. Fire, 2024, 7(8), 278. https://doi.org/10.3390/fire7080278
24. Mutthulakshmi, K., Wee, M. R. E., Wong, Y. C. K., Lai, J. W., Koh, J. M., Acharya, U. R., Cheong, K. H. Simulating Forest Fire Spread and Fire-Fighting Using Cellular Automata. Chinese Journal of Physics, 2020, 65, 642-650. https://doi.org/10.1016/j.cjph.2020.04.001
25. Pereira, J., Mendes, J., Júnior, J., Carlos Viegas, João Ruivo Paulo. Metaheuristic Algorithms for Calibration of Two-Dimensional Wildfire Spread Prediction Model. Engineering Applications of Artificial Intelligence, 2024, 136, 108928. https://doi.org/10.1016/j.engappai.2024.108928
26. Prema, C., Vinsley, S. S., Suresh, S. Efficient Flame Detection Based on Static and Dynamic Texture Analysis in Forest Fire Detection. Fire Technology, 2018, 54, 255-288. https://doi.org/10.1007/s10694-017-0683-x
27. Roh, J., Kim, Y., Kong, M. Fire Image Classification Based on Convolutional Neural Network for Smart Fire Detection. International Journal of Fire Science and Engineering, 2022, 36(3), 51-61. https://doi.org/10.7731/KIFSE.cb750817
28. San-Miguel-Ayanz, J., Ravail, N. Active Fire Detection for Fire Emergency Management: Potential and Limitations for the Operational Use of Remote Sensing. Natural Hazards, 2005, 35, 361-376. https://doi.org/10.1007/s11069-004-1797-2
29. Schultze, T., Kempka, T., Willms, I. Audio-Video Fire-Detection of Open Fires. Fire Safety Journal, 2006, 41(4), 311-314. https://doi.org/10.1016/j.firesaf.2006.01.002

30. Taranchuk, V. B. Intelligent Computing, Cognitive Graphics, Neural Networks in Computer Models of Forest Fires. In 21st International Workshop on Computer Science and Information Technologies (CSIT 2019). Atlantis Press, 2019, 317-321. https://doi.org/10.2991/csit-19.2019.55

31. Ujjwal, K. C., Aryal, J., Garg, S., Hilton, J. Global Sensitivity Analysis for Uncertainty Quantification in Fire Spread Models. Environmental Modelling & Software, 2021, 143, 105110. https://doi.org/10.1016/j.envsoft.2021.105110

32. Wu, S., Sheng, B., Fu, G., Zhang, D., Jian, Y. Multiscale Fire Image Detection Method Based on CNN and Transformer. Multimedia Tools and Applications, 2024, 83(16), 49787-49811. https://doi.org/10.1007/s11042-023-17482-4

33. Zhang, S., Liu, J., Gao, H., Chen, X., Li, X., Hua, J. Study on Forest Fire Spread Model of Multi-Dimensional Cellular Automata Based on Rothermel Speed Formula. Cerne, 2022, 27, e-102932. https://doi.org/10.1590/01047760202127012932

34. Zhao, L., Zhi, L., Zhao, C., Zheng, W. Fire-YOLO: A Small Target Object Detection Method for Fire Inspection. Sustainability, 2022, 14, 4930. https://doi.org/10.3390/su14094930

35. Zheng, Z., Huang, W., Li, S., Zeng, Y. Forest Fire Spread Simulating Model Using Cellular Automaton with Extreme Learning Machine. Ecological Modelling, 2017, 348, 33-43. https://doi.org/10.1016/j.ecolmodel.2016.12.022